SCIENTIFIC REPORTS
nature research

Check for updates

OPEN

Pd on poly(1-vinylimidazole) decorated magnetic S-doped grafitic carbon nitride: an efficient catalyst for catalytic reduction of organic dyes

Masoumeh Dorraj[1], Samahe Sadjadi[1]✉ & Majid M. Heravi[2]

A novel magnetic catalyst, (SGCN/Fe_3O_4/PVIs/Pd) was synthesized by growing of poly(1-vinylimidazole) on the surface of ionic liquid decorated magnetic S-doped graphitic carbon nitride, followed by stabilization of palladium nanoparticles. Catalytic activity of the prepared heterogeneous catalyst was explored for the catalytic reduction of hazardous dyes, methyl orange and Rhodamine B, in the presence of $NaBH_4$. Besides, the effects of the reaction variables on the catalytic activity were investigated in detail. The kinetics study established that dye reduction was the first order reaction and the apparent activation energy was calculated to be 72.63 kJ/mol and 68.35 kJ/mol^1 for methyl orange and Rhodamine B dyes, respectively. Moreover, $\Delta S^{\#}$ and $\Delta H^{\#}$ values for methyl orange were found to be − 33.67 J/mol K and 68.39 kJ/mol respectively. These values for Rhodamine B were − 45.62 J/mol K and 65.92 kJ/mol. The recycling test verified that the catalyst possessed good stability and reusability, thereby making it a good candidate for the catalytic purposes. Furthermore, a possible catalytic mechanism for dye catalytic reduction over SGCN/Fe_3O_4/PVIs/Pd was proposed.

Dyes and pigments are widely used in cosmetics, textiles, paper, printing and many other industries. It is thus not surprising that organic dyes such as methyl orange (MO) and Rhodamine B(RhB) are one of the most common anthropogenic water pollutants in industrial effluent. Most of these compounds are acutely toxic, mutagenic and either known or suspected carcinogens[1,2]. Many technologies have been designed for the treatment of wastewater containing organic dyes, including adsorption[3], coagulation[3,4] and reverse osmosis[5]. However, the mentioned methods are not sufficient and effective for dye catalytic reduction to nonhazardous products[6]. As a consequence, searching for an effective and suitable approach for the efficient removal of dyes is extremely essential. Chemical reduction method in the presence of metal nanoparticles and $NaBH_4$ is considered to be a feasible and potential approach for dye decolonization due to its advantages of low-cost, high-efficiency, and easy operation[7,8].

Noble metal based nanomaterials have recently gained significant attention, since they have outstanding physicochemical properties and great potentials in various fields such as optical, catalytic, biomedical and environmental application[9–12]. Among them, palladium nanoparticles (Pd NPs) are the most promising nanoparticles served in several industries and academic synthetic chemistry laboratories as effective catalysts for many organic reactions[13]. However, in the practical application, noble metal NPs can agglomerate easily because of their large surface area, which subsequently results in poor catalytic activity and durability[13–15].

To solve this problem, a large number of supporting materials, such as polymers[12,16], metal oxides[17–20], clays[21] and carbon based materials[22–24] have been used to support and stabilize NPs. Among many types of carbon based support, graphitic carbon nitride (g-C_3N_4) has been considered as an ideal support for various metal nanoparticles[25–29]. However, the pristine g-C_3N_4, still suffers from unsatisfactory adsorption performance owing to its insufficient active sites and limited specific surface area. An important strategy for improving the adsorption capacity of g-C_3N_4 is enhancing the active sites by doping heteroatoms (e.g. S, O, B, P)[30–33]. In addition, the

[1]Gas Conversion Department, Faculty of Petrochemicals, Iran Polymer and Petrochemicals Institute, PO Box 14975-112, Tehran, Iran. [2]Department of Chemistry, School of Science, Alzahra University, Vanak, PO Box 1993891176, Tehran, Iran. ✉email: s.sadjadi@ippi.ac.ir

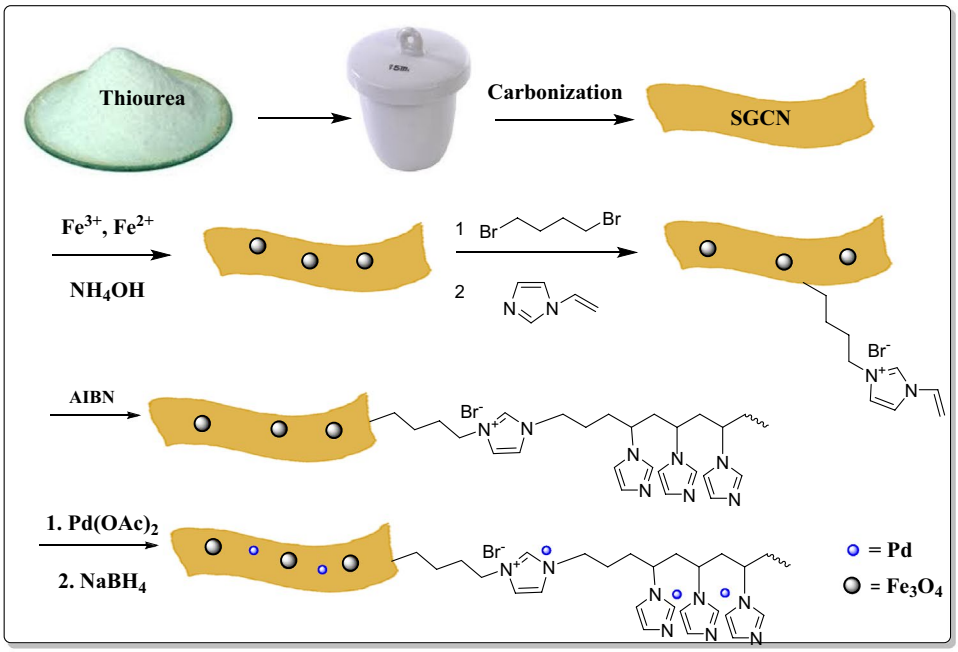

Figure 1. The schematic procedure of the synthesis of the SGCN/Fe_3O_4/PVIs/Pd catalyst.

element doping approach can increase some defects of bulk g-C_3N_4[34,35], thus providing more active sites for binding target ions. Among doped g-C_3N_4, S-g-C_3N_4 (SGSN) showed improved electron transfer and catalytic performance[36,37]. For example, Li et al.[33] showed that doping g-C_3N_4 with S can facilitate the adsorption ability of Pb(II) since soft S ligands serve as Pb(II) scavenger. Thus, use of SGCN can improve the performance of graphitic carbon as a support.

Magnetic nanoparticles offer significant promise due to their magnetic properties, allowing for easy and fast recovery with a conventional magnet[38,39]. Therefore, the design and development of new magnetic catalysts that can be easily separated from the solution is of great importance.

One of the major problems associated with the immobilized metallic heterogeneous catalysts is the low catalyst loading and high catalyst leaching. In the conventional immobilization of metal NPs on a solid support, only one layer of the support surface is available and consequently the metal loading is expected to be low. This problem can be addressed by coating of solid surfaces by functional polymers[17,40,41]. Among various functional polymers, poly (1-vinylimidazole) (PVI) has been intensively studied as a compound for anchoring metal ions in solution. In some cases, PVI has been employed due to its complex formation capability[42], whereas other studies focused on the utility of PVI for the preparation of polymer-grafted nanoparticles[41]. Vinylimidazole (VI) has also been successfully used for the synthesis an ion-imprinted silica supported organic–inorganic hybrid for heavy metal ions removal[43] and carrying metal-chelated beads for reversible use in yeast invertase adsorption[44].

Ionic liquids, ILs, are a class of very applicable organic salts that can be applied as catalysts, carbon precursor and solvents[45–47]. These organic salts can also be successfully used for the immobilization of catalytic species on the supports[48].

In the pursuit of our research on the design of novel hybrid catalytic systems based on g-C_3N_4[49–51] and IL[52–54], herein, we report the synthesis of a novel magnetic heterogeneous hybrid catalyst. In this catalytic system, magnetic SGSN was functionalized with vinyl IL and then polymerized with vinyl imidazole to form PVI. The resulting hybrid was then applied as a support for Pd immobilization, (Fig. 1). The prepared SGCN/Fe_3O_4/PVIs/Pd nanocomposite was then used as a magnetic catalyst for the catalytic reduction of MO and RhB in the presence of $NaBH_4$. In addition, the kinetic and the effects of the reaction temperature, the catalyst amount and the reaction time on the removal of MO and RhB were investigated. Moreover, the recyclability of SGCN/Fe_3O_4/PVIs/Pd was studied.

Result and discussion

Catalyst characterizations. The X-ray diffraction (XRD) was applied to monitor the crystal phase of SGCN (Fig. S1) and SGCN/Fe_3O_4/PVIs/Pd (Fig. 2). Typically, the strongest peak observed for SGCN at $2\theta = 27.6°$ can be representative of interlayer stacking of aromatic system (002). A small diffraction peak at $2\theta = \sim 13.1°$ can be indexed to the (100) plane and assigned to the in-plane aromatic structural packing[33,55]. Regarding SGCN/Fe_3O_4/PVIs/Pd nanocomposite XRD pattern, the peak at $2\theta = 27.6°$ had a considerably reduced intensity and became broader, while the peak at 13.1° vanished, owing to the introduction of Fe_3O_4, Pd NPs or the interaction of the Pd NPs and SGCN in SGCN/Fe_3O_4/PVIs/Pd nanocomposite[33,38]. Eleven characteristic diffraction peaks of Fe_3O_4 are found in XRD pattern of SGCN/Fe_3O_4/PVIs/Pd nanocomposite (denoted as black circles)[56], suggest-

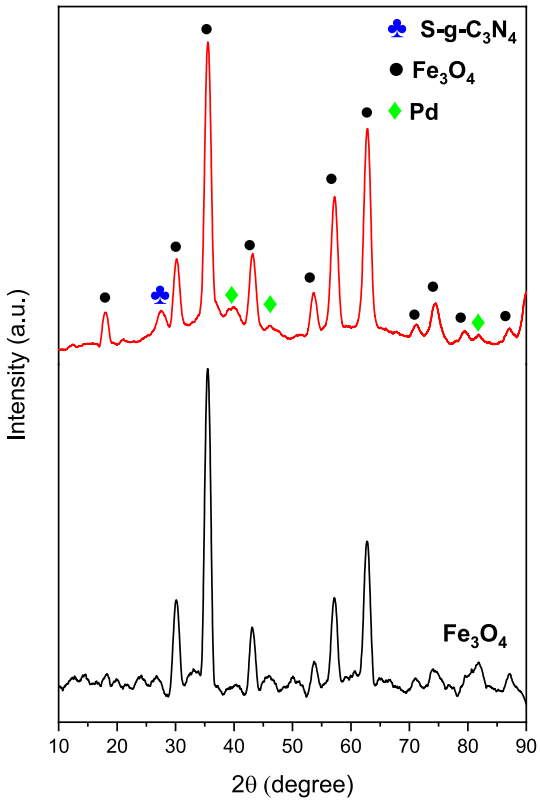

Figure 2. XRD pattern of SGCN/Fe_3O_4/PVIs/Pd nanocomposite.

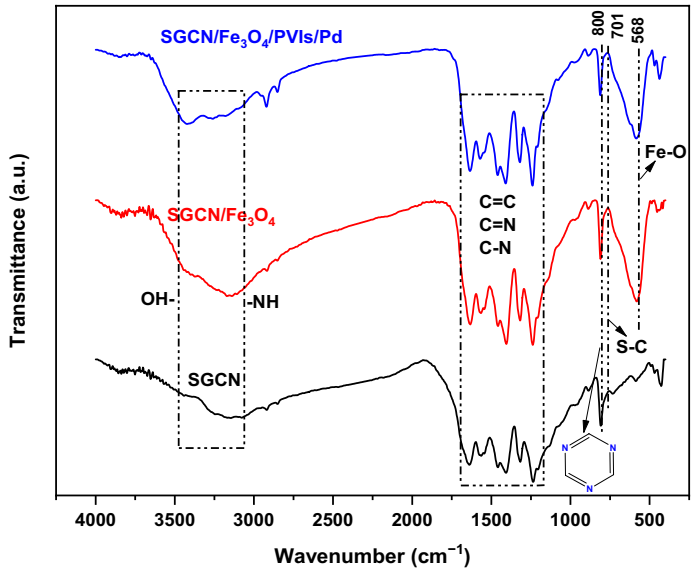

Figure 3. FT-IR spectra of SGCN, SGCN/Fe_3O_4 and SGCN/Fe_3O_4/PVIs/Pd nanocomposite.

ing that Fe_3O_4 has been successfully immobilized on S-g-C_3N_4. The indexed (111) and (200) diffraction peaks at 39.66°, 46.46° and 82.08° are assigned to the Pd NPs (JCPDS No. 46–1,043), corresponding to the face centered cubic (fcc) Pd lattices[57].

The FTIR spectra of SGCN, SGCN/Fe_3O_4 and SGCN/Fe_3O_4/PVIs/Pd nanocomposite are presented in Fig. 3. FTIR spectra of all the above mentioned materials presented similar absorption bands at 800 and 1,200–1,600 cm^{-1}, which are attributed to triazine units, aromatic –C=C/–C=N/–C–N bonds, as well as the band at 3,100–3,500 cm^{-1} that can be assigned to –NH and –OH groups[30,33]. The presence of S–C bond at 701 cm^{-1}

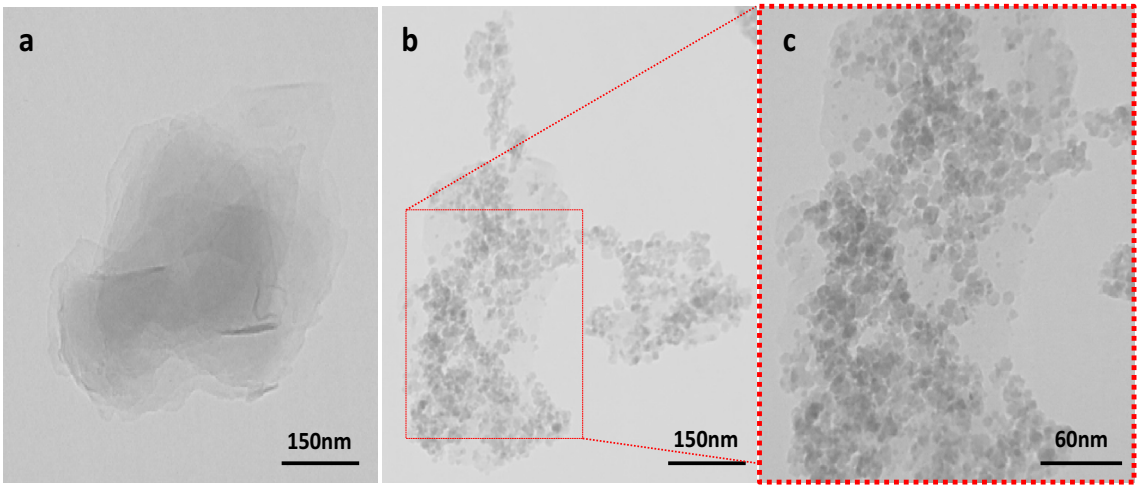

Figure 4. TEM images of (**a**) SGCN and (**b**, **c**) SGCN/Fe_3O_4/PVIs/Pd nanocomposite.

in the FTIR spectrum of SGCN, implied the successful incorporation of sulfur into g-C_3N_4 structure[33,37]. As for SGCN/Fe_3O_4 and SGCN/Fe_3O_4/PVIs/Pd, the absorption band at 568 cm^{-1} can be due to Fe–O bond[38].

The morphologies of SGCN and SGCN/Fe_3O_4/PVIs/Pd samples were examined with TEM as shown in Fig. 4a–c. Figure 4a shows the film-like morphology with a layered structure of the SGCN (a unique folded graphene like structure composed of spatially interconnected nanosheets). Figure 4b,c corroborated that Fe_3O_4 and Pd nanoparticles are highly dispersed on the surface of the support. Furthermore, the EDS analysis of SGCN/Fe_3O_4/PVIs/Pd nanocomposite (Fig. S2) showed the presence of Fe and Pd atoms, affirming successful incorporation of metallic nanoparticles on the hybrid support. Moreover, the presence of S, C and N is indicative of SGCN. Notably, the absence of Br atom can be ascribed to its low content.

FESM image and elemental mapping analysis of SGCN/Fe_3O_4/PVIs/Pd nanocomposite were also recorded, Fig. S3. It was found that both Pd and magnetic nanoparticles were dispersed homogeneously on the composite.

Magnetic properties of the Fe_3O_4 and SGCN/Fe_3O_4/PVIs/Pd samples were investigated at room temperature, Fig. S4. It was confirmed that the magnetization saturation of SGCN/Fe_3O_4/PVIs/Pd was 38.42 emu/g, lower than that of Fe_3O_4 (51.3 emu/g). This result can be justified by considering the fact that Fe_3O_4 nanoparticles were embedded in the support that is a non-magnetic compound[58].

Fig. S5 showed the thermogravimetric analysis (TGA) results of SGCN and SGCN/Fe_3O_4/PVIs/Pd. As for SGCN, upon increase of temperature up to 550 °C, the sublimation or decomposition of SGCN initiated. This process is completed at 650 °C. For SGCN/Fe_3O_4/PVIs/Pd nanocomposite, however, the stability of the nanocomposites greatly decreased (the decomposition temperature is shifted to 449.1 °C, which is lower than that of SGCN). This is assigned to the oxidation and decomposition of PVIs.

Kinetic and thermodynamic studies of the reduction reaction of dyes in the presence of SGCN/Fe_3O_4/PVIs/Pd catalyst. The catalytic activity of the SGCN/Fe_3O_4/PVIs/Pd nanocomposite was evaluated in the reduction reaction of MO and RhB dyes with $NaBH_4$ as the reducing agent and the progress of reaction monitored with the help of ultraviolet–visible (UV–Vis) absorption spectroscopy. The initial experiments established that in the absence of the catalyst, no reaction progress was apperceived, indicating that the catalyst play an important role in the reduction process. In the next step, the influence of SGCN/Fe_3O_4/PVIs/Pd loading on MO and RhB catalytic reduction was assessed. In this regard, the catalytic performances of different amounts of catalyst (1, 2, 3, 4 and 5 mg) were evaluated under similar operating condition (performing the reaction at room temperature, in water as solvent). Experimental results affirmed that the conversion of the reactions increased by the increment of the content of SGCN/Fe_3O_4/PVIs/Pd up to an optimum level (2 mg for MO and 4 mg for RhB) and further increase of SGCN/Fe_3O_4/PVIs/Pd loading had no remarkable effect on the reaction conversion, Table S1.

The reduction progress for both dyes over time was monitored by measuring the temporal evolution of UV–Vis absorption spectra of the reaction mixtures under SGCN/Fe_3O_4/PVIs/Pd catalysis (Fig. 5). As shown, the absorption peaks of the dyes (λ_{max} = 465 nm for MO and λ_{max} = 550 nm for RhB) decreased gradually as the reaction elapsed. This implied high efficiency of SGCN/Fe_3O_4/PVIs/Pd for dye decolorization in a short time of the reaction (40 s for MO and 50 s for RhB).

The MO and RhB catalytic reduction processes followed the pseudo-first-order kinetic, which can be described by the following equation[59,60]:

$$\ln {}^{C_0}/_{C} = kt \quad (1)$$

In that equation, the values of C_0 (dye concentration at the start of the reaction) and C (dye concentration at time t) can be obtained from the absorbance at t = 0 and t (A_0 and A_t) respectively. Hence, the values of the rate constant (k) for the reduction of dyes can be calculated from the slope of ln (C_0/C) vs. time (Fig. S6).

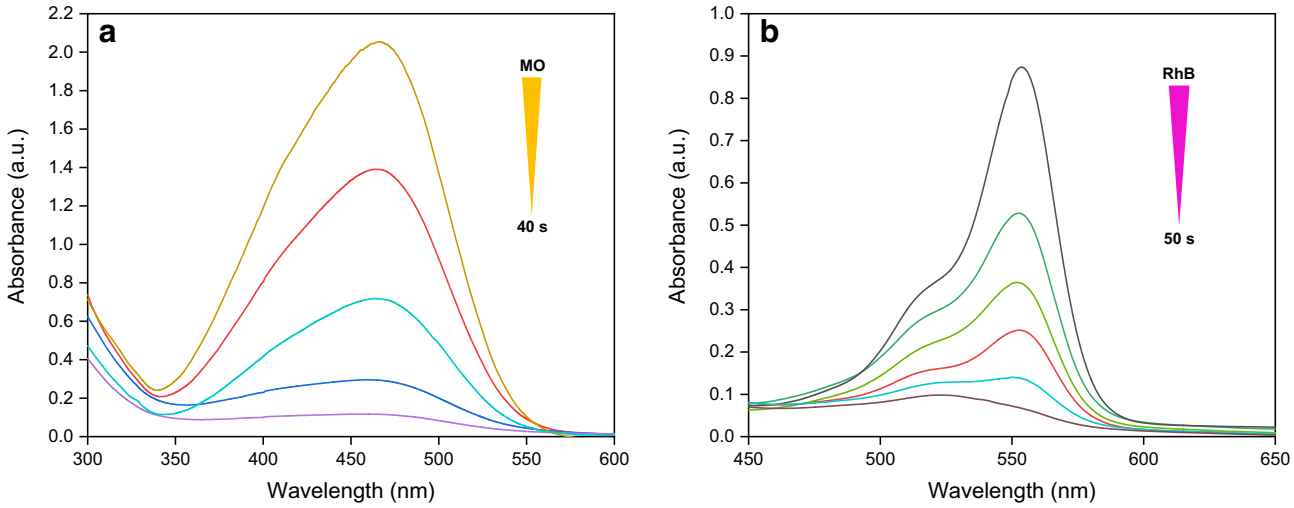

Figure 5. Time-dependent UV–visible spectra for the catalytic reduction of (**a**) MO and (**b**) RhB dyes by $NaBH_4$ in the presence of optimum amount of SGCN/Fe_3O_4/PVIs/Pd.

Dye	T (K)	k (min^{-1})	E_a (kJ/mol)	$\Delta S^{\#}$ (J/mol K)	$\Delta H^{\#}$ (kJ/mol)
MO	293 298 303 308	0.036 0.052 0.115 0.141	72.63	33.67	68.39
RhB	293 298 303 308	0.040 0.080 0.124 0.154	68.35	45.62	5.92

Table 1. The values of thermodynamic and kinetic parameters of reduction reaction of MO and RhB dyes in the presence of the SGCN/Fe_3O_4/PVIs/Pd catalyst.

The k values for the reduction of both MO and RhB at four different reaction temperatures (293, 298, 303 and 308 K) were similarly measured, reported in Table 1. As tabulated, k value of the reaction increased with the increment of the reaction temperature (Table 1). k values at different temperatures can be helpful for estimating the activation energies (E_a). More exactly, having the Arrhenius equation in hand, Eq. (2), and R and k values, E_a can be measured from the plot of ln k vs. 1/T as shown in Fig. S7 and Table 1.

$$\ln k = \ln A - \left(E_a/RT\right) \tag{2}$$

For the calculation of activation thermodynamics parameters, i.e. activation entropy ($\Delta S^{\#}$) and the activation enthalpy ($\Delta H^{\#}$), Eyring equation (Eq. 3) and Eyring plot (ln (k/T) vs. 1/T), Fig. S8, were exploited.

$$\ln\left(k/T\right) = \ln\left(k_B/h\right) + \Delta S^{\#}/R - \Delta H^{\#}/R\left(1/T\right) \tag{3}$$

In Eq. (3), k_B and h are constant and known values. Moreover, the study of the kinetic parameters provided the value of ln (k/T). Hence, $\Delta S^{\#}$ and $\Delta H^{\#}$ can be evaluated from the intercept and slop of Eyring plot respectively. The measured $\Delta S^{\#}$ values for the reduction reactions of MO and RhB were assessed as -33.678 and −45.626 J/mol K, respectively. $\Delta H^{\#}$ values of the reduction reactions were measured as 68.397 and 65.929 kJ/mol for MO and RhB dyes, respectively (Table 1).

Mechanism. According to the literature[61], the plausible mechanism for the reduction of MO and RhB in the presence of SGCN/Fe_3O_4/PVIs/Pd can be defined as follow: First, borohydride ions are generated through dissociation of sodium borohydride. Secondly, the as-generated BH_4^- ions are adsorbed on Pd nanoparticles that are the main catalytic species for the reduction reaction. On the other hand, the organic dyes that possess aromatic moieties in their structures can be adsorbed onto SGCN/Fe_3O_4/PVIs/Pd through π-π stacking interactions. Thirdly, the adsorbed dyes were reduced by the generated hydride ions, Fig. 6. Finally, the reduced dye will be released from SGCN/Fe_3O_4/PVIs/Pd.

Recyclability. Considering the importance of the reuse of the heterogeneous catalysts in the practical application, the recyclability of SGCN/Fe_3O_4/PVIs/Pd for the reduction reaction of both dyes was examined.

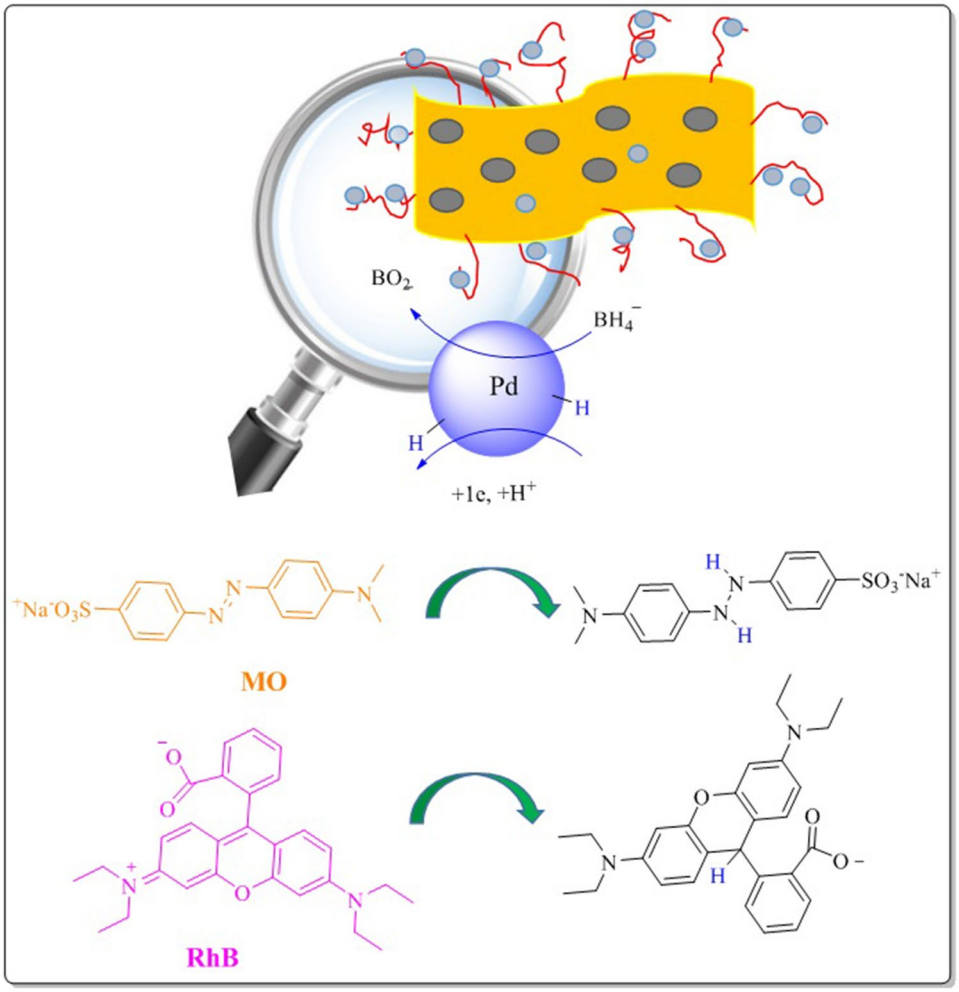

Figure 6. The plausible mechanism for dye reduction.

To accomplish this purpose, SGCN/Fe_3O_4/PVIs/Pd was separated by applying an external magnetic from the reaction mixture and then employed for the next reaction run under the same reaction condition. This cycle was repeated up to eight consecutive reaction runs and the obtained yields of each runs for both dyes were measured and compared (Fig. 7). As shown in Fig. 7, SGCN/Fe_3O_4/PVIs/Pd could be recycled for 8 reaction runs with only slight loss of the catalytic activity. Furthermore, the Pd leaching of SGCN/Fe_3O_4/PVIs/Pd was also investigated for the catalyst reused after eight runs. It was gratifyingly found out that Pd leaching was insignificant (0.01 wt% of initial Pd loading), showing the efficiency and stability of SGCN/Fe_3O_4/PVIs for Pd anchoring.

Next, the stability of the recycled SGCN/Fe_3O_4/PVIs/Pd was evaluated by recording FTIR spectrum of the recycled SGCN/Fe_3O_4/PVIs/Pd after eight runs for the reduction of MO and RhB (Fig. S9a). It was found that the spectra of the recycled SGCN/Fe_3O_4/PVIs/Pd for both reactions are similar to that of fresh SGCN/Fe_3O_4/PVIs/Pd and no absorbance band has been disappeared upon recycling. Moreover, the TEM analysis of the recycled catalyst after eight cycles did not show major morphological changes (Fig. S9b). These implied that the structure and morphology of SGCN/Fe_3O_4/PVIs/Pd were not destroyed after recycling.

Experimental

The detail of used materials and apparatus is elaborated in SI. Herein, the syntheses of the catalyst and dye reduction are explained.

Synthesis of the catalyst. *Synthesis of S-g-C_3N_4 nanosheet (SGCN).* Sulphur-doped graphitic carbon nitride (S-g-C_3N_4) nanosheets were synthesized by carbonization of thiourea in a muffled furnace[30]. In brief, 10 g of thiourea was placed in crucibles with a cover and calcined at 530 °C in a muffle furnace for 2 h. After calcination, the obtained yellow powder marked as SGCN was ground into fine powder and collected for further usage.

Synthesis of the SGCN/Fe_3O_4. SGCN/Fe_3O_4 nanocomposites was synthesized by precipitation method[6]. Briefly, SGCN powder (0.5 g) was added to 120 mL of distilled water and ultrasonicated (60 W) for 20 min at room

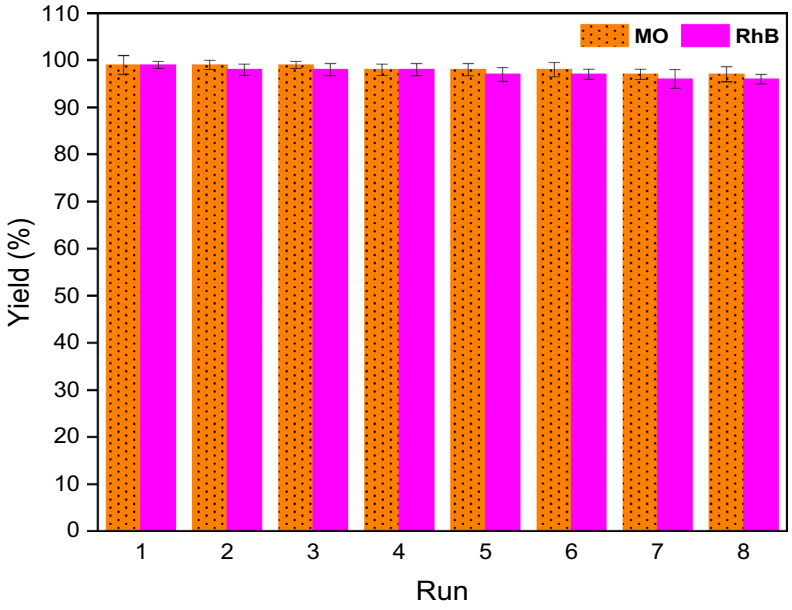

Figure 7. The results of the recyclability of the catalyst for reduction of MO and RhB.

temperature. Then, $FeCl_3.6H_2O$ (1.37 g) and $FeCl_2{\cdot}4H_2O$ (0.5 g) were dissolved into 12 mL distilled water and the resultant solutions were added to the SGCN suspension under stirring. Stirring was continued for 60 min at 80 °C, and then 10 mL of ammonia solution was added and the mixture was continuously stirred for 60 min, after which the suspension was allowed to cool naturally. Then, the as prepared precipitate was collected by an external magnet, washed with water and ethanol, and dried at 50 °C overnight. The obtained product (named as SGCN/Fe_3O_4) was used in the next step.

Synthesis of SGCN/Fe_3O_4/PVIs Hybrids. SGCN/Fe_3O_4 (1.0 g) was dispersed in 45 mL toluene in a clean round-bottom flask. Subsequently, 1,4-dibromobutane (1 mL) was added to the stirring mixture. The resulting mixture was heated, refluxed and kept at 110 °C for 24 h under vigorous agitation. At the end of the reaction, the product was subjected to magnetic separation and washed sequentially with EtOH to thoroughly remove unreacted 1,4-dibromobutane from the surface of SGCN/Fe_3O_4. The final product, denoted as SGCN/Fe_3O_4 -$(CH_2)_4$Br, was then dried under vacuum at 60 °C overnight to remove the residual solvent. To introduce IL, a mixture containing SGCN/Fe_3O_4-$(CH_2)_4$Br (1.0 g) and 1-vinylimidazole (1.5 mL) in 35.0 mL EtOH was stirred for 15 min and then refluxed at 60 °C for 3 h under vigorous agitation to form SGCN/Fe_3O_4-$(CH_2)_4$IL. Growth of poly (1-vinylimidazole) (PVI) was achieved via free radical polymerization of 1-vinylimidazole and SGCN/Fe_3O_4-$(CH_2)_4$IL in the presence of AIBN (50 mg) as initiator. Polymerization was continued at 80 °C for 24 h under Ar atmosphere. Upon completion of the polymerization reaction, the product was separated magnetically and then washed with ethanol several times. The produced SGCN/Fe_3O_4/ PVIs was dried under vacuum at 60 °C to remove the residual solvent.

Preparations of SGCN/Fe_3O_4/PVIs/Pd. Stabilization of Pd nanoparticles was realized through wet-impregnation procedure[15]. 1.2 g of the SGCN/Fe_3O_4/PVIs was agitated in 50 mL toluene. Afterwards, a solution of 0.1 mmol of $Pd(OAc)_2$ in 20 mL of toluene was added gradually. After agitation at room temperature for 2 h, a solution sodium borohydride in H_2O (10 mL, 0.2 N), was added to provide Pd(0) nanoparticles. At the end, SGCN/Fe_3O_4/PVIs/Pd was collected, washed with MeOH /EtOH, and dried under vacuum for 13 h. Figure 1 present a schematic illustration of preparation of SGCN/Fe_3O_4/PVIs/Pd. Using ICP method, Pd loading was measured as 0.07 $mmolg^{-1}$.

Catalytic reduction of dye. To decolorize the dyes, MO or RhB (2 mL), scan content of SGCN/Fe_3O_4/PVIs/Pd and sodium borohydride (2 mL, 0.01 M) were mixed in water and stirred. The progress of de-colorization was traced by using time-dependent UV–vis spectroscopy[61]. At the end of the reaction, SGCN/Fe_3O_4/PVIs/Pd was collected, rinsed repeatedly with EtOH: H_2O (1:1) and dried. This experiment was repeated at four temperatures (20, 25, 30 and 35 °C).

Conclusion

In summary, growth of PVI on IL decorated magnetic SGCN has been reported to furnish an efficient support for stabilization of Pd NPs. The resulting catalyst, SGCN/Fe_3O_4/PVIs/Pd, was characterized and applied for the catalytic reduction of MO and RhB in aqueous media at room temperature. The results confirmed high efficiency of the catalyst for reduction of both dyes in almost 1 min, probably because of the chelation properties. The

study of the reaction temperature confirmed that the higher the reaction temperature, the faster the reaction proceeded. Moreover, the effect of the catalyst loading was studied to find out the optimum catalyst loading for both reactions. The rate constants of both reactions were calculated at four different temperatures and using some conventional calculation, E_a, $\Delta S^{\#}$ and $\Delta H^{\#}$ values for MO were found to be 68.35 kJ/mol, − 33.67 J/mol K and 68.39 kJ/mol respectively. These values for RhB were 72.63 kJ/mol, − 45.62 J/mol K and 65.92 kJ/mol. Moreover, the recycling of SGCN/Fe_3O_4/PVIs/Pd confirmed facile recovery of the catalyst and its excellent recyclability up to eight runs. This catalyst has good potential to real-life applications because of easy handling and separation, and long-term stability. In fact, in this study the chemistry of graphitic carbon nitride was modified by incorporation of heteroatom and introduction of PVI to furnish a potential support for Pd immobilization and developing a catalyst for removal of dyes.

Received: 6 June 2020; Accepted: 24 July 2020
Published online: 10 August 2020

References

1. Kurtan, U., Baykal, A. & Sözeri, H. Recyclable Fe_3O_4@ Tween20@ Ag nanocatalyst for catalytic degradation of azo dyes. *J. Inorg. Organomet.* **25**, 921–929 (2015).
2. Saravanan, R., Gupta, V. K., Prakash, T., Narayanan, V. & Stephen, A. Synthesis, characterization and photocatalytic activity of novel Hg doped ZnO nanorods prepared by thermal decomposition method. *J. Mol. Liq.* **178**, 88–93 (2013).
3. Lee, J.-W., Choi, S.-P., Thiruvenkatachari, R., Shim, W.-G. & Moon, H. Evaluation of the performance of adsorption and coagulation processes for the maximum removal of reactive dyes. *Dyes Pigments* **69**, 196–203 (2006).
4. Golob, V., Vinder, A. & Simonič, M. Efficiency of the coagulation/flocculation method for the treatment of dyebath effluents. *Dyes Pigments* **67**, 93–97 (2005).
5. Kim, T.-H., Park, C. & Kim, S. Water recycling from desalination and purification process of reactive dye manufacturing industry by combined membrane filtration. *J. Clean. Prod.* **13**, 779–786 (2005).
6. Radoń, A., Drygała, A., Hawełek, Ł & Łukowiec, D. Structure and optical properties of Fe_3O_4 nanoparticles synthesized by co-precipitation method with different organic modifiers. *Mater. Charact.* **131**, 148–156 (2017).
7. Li, B., Hao, Y., Zhang, B., Shao, X. & Hu, L. A multifunctional noble-metal-free catalyst of CuO/TiO_2 hybrid nanofibers. *Appl. Catal. A* **531**, 1–12 (2017).
8. Li, B. *et al.* Understanding size-dependent properties of BiOCl nanosheets and exploring more catalysis. *J. Colloid Interface Sci.* **505**, 653–663 (2017).
9. Li, J. *et al.* Engineering noble metal nanomaterials for environmental applications. *Nanoscale* **7**, 7502–7519 (2015).
10. Saha, K., Agasti, S. S., Kim, C., Li, X. & Rotello, V. M. Gold nanoparticles in chemical and biological sensing. *Chem. Rev.* **112**, 2739–2779 (2012).
11. Sadjadi, S., Heravi, M. M. & Malmir, M. Bio-assisted synthesized Ag (0) nanoparticles immobilized on SBA-15/cyclodextrin nanosponge adduct: Efficient heterogeneous catalyst for the ultrasonic-assisted synthesis of benzopyranopyrimidines. *Appl. Organomet. Chem.* **32**, e4286 (2018).
12. Sadjadi, S., Ghoreyshi Kahangi, F., Dorraj, M. & Heravi, M. M. Ag nanoparticles stabilized on cyclodextrin polymer decorated with multi-nitrogen atom containing polymer: an efficient catalyst for the synthesis of xanthenes. *Molecules* **25**, 241 (2020).
13. Nandi, D., Siwal, S., Choudhary, M. & Mallick, K. Carbon nitride supported palladium nanoparticles: an active system for the reduction of aromatic nitro-compounds. *Appl. Catal. A* **523**, 31–38 (2016).
14. Sadjadi, S., Akbari, M. & Heravi, M. M. Palladated nanocomposite of halloysite–nitrogen-doped porous carbon prepared from a novel cyano-/nitrile-free task specific ionic liquid: an efficient catalyst for hydrogenation. *ACS omega* **4**, 19442–19451 (2019).
15. Sadjadi, S., Akbari, M., Léger, B., Monflier, E. & Heravi, M. M. Eggplant-derived biochar-halloysite nanocomposite as supports of Pd nanoparticles for the catalytic hydrogenation of nitroarenes in the presence of cyclodextrin. *ACS Sustain. Chem. Eng.* **7**, 6720–6731 (2019).
16. Sadjadi, S., Heravi, M. M. & Raja, M. Composite of ionic liquid decorated cyclodextrin nanosponge, graphene oxide and chitosan: a novel catalyst support. *Int. J. Biol. Macromol.* **122**, 228–237 (2019).
17. Veisi, H., Kamangar, S. A., Mohammadi, P. & Hemmati, S. Palladium nanoparticles-decorated triethanolammonium chloride ionic liquid-modified TiO_2 nanoparticles (TiO_2/IL-Pd): a highly active and recoverable catalyst for Suzuki-Miyaura cross-coupling reaction in aqueous medium. *Appl. Organomet. Chem.* **33**, e4909 (2019).
18. Mohammadi, P. & Sheibani, H. Synthesis and characterization of Fe_3O_4@ SiO_2 guanidine-poly acrylic acid nanocatalyst and using it for one-pot synthesis of 4H-benzo [b] pyrans and dihydropyrano [c] chromenes in water. *Mater. Chem. Phys.* **228**, 140–146 (2019).
19. Pourjavadi, A., Keshavarzi, N., Moghaddam, F. M. & Hosseini, S. H. Immobilization of nickel ions onto the magnetic nanocomposite based on cross-linked melamine groups: effective heterogeneous catalyst for N-Arylation of Arylboronic acids. *Appl. Organomet. Chem.* **32**, e4107 (2018).
20. Xiao, Y., He, Z., Wang, R., Tao, X. & Li, B. Synthesis of WO_3 nanofibers decorated with BiOCl nanosheets for photocatalytic degradation of organic pollutants under visible light. *Colloids Surf. A* **580**, 123752 (2019).
21. Sadjadi, S., Akbari, M. & Heravi, M. M. Palladated nanocomposite of halloysite-nitrogen-doped porous carbon prepared from a novel cyano-/nitrile-free task specific ionic liquid: an efficient catalyst for hydrogenation. *ACS Omega* **4**, 19442–19451 (2019).
22. Chen, P., Chew, L. M., Kostka, A., Muhler, M. & Xia, W. The structural and electronic promoting effect of nitrogen-doped carbon nanotubes on supported Pd nanoparticles for selective olefin hydrogenation. *Catal. Sci.* **3**, 1964–1971 (2013).
23. Torres-Mendieta, R. *et al.* In situ decoration of graphene sheets with gold nanoparticles synthetized by pulsed laser ablation in liquids. *Sci. Rep.* **6**, 30478 (2016).
24. Ren, F. *et al.* Clean method for the synthesis of reduced graphene oxide-supported PtPd alloys with high electrocatalytic activity for ethanol oxidation in alkaline medium. *ACS Appl. Mater. Interfaces* **6**, 3607–3614 (2014).
25. Mohammadi, L., Heravi, M. M., Sadjadi, S. & Malmir, M. Hybrid of graphitic carbon nitride and palladated magnetic carbon dot: an efficient catalyst for coupling reaction. *ChemistrySelect* **4**, 13404–13411 (2019).
26. Sun, J., Fu, Y., He, G., Sun, X. & Wang, X. Green Suzuki-Miyaura coupling reaction catalyzed by palladium nanoparticles supported on graphitic carbon nitride. *Appl. Catal. B* **165**, 661–667 (2015).
27. Fu, Y., Huang, T., Zhang, L., Zhu, J. & Wang, X. Ag/g-C_3N_4 catalyst with superior catalytic performance for the degradation of dyes: a borohydride-generated superoxide radical approach. *Nanoscale* **7**, 13723–13733 (2015).
28. Xiao, Y. *et al.* Optimal synthesis of a direct Z-scheme photocatalyst with ultrathin $W_{18}O_{49}$ nanowires on g-C_3N_4 nanosheets for solar-driven oxidation reactions. *J. Colloid Interface Sci.* **550**, 99–109 (2019).
29. Xiao, Y. *et al.* Synthesis of EDTA-bridged CdS/g-C_3N_4 heterostructure photocatalyst with enhanced performance for photoredox reactions. *J. Colloid Interface Sci.* **577**, 459–4570 (2020).

30. Zhang, J. *et al.* Sulfur-mediated synthesis of carbon nitride: band-gap engineering and improved functions for photocatalysis. *Energy Environ. Sci.* **4**, 675–678 (2011).
31. Zhang, Y., Mori, T., Ye, J. & Antonietti, M. Phosphorus-doped carbon nitride solid: enhanced electrical conductivity and photocurrent generation. *J. Am. Chem. Soc.* **132**, 6294–6295 (2010).
32. Zou, Y. *et al.* β-Cyclodextrin modified graphitic carbon nitride for the removal of pollutants from aqueous solution: experimental and theoretical calculation study. *J. Mater. Chem. A* **4**, 14170–14179 (2016).
33. Li, X. *et al.* Adsorption of lead on sulfur-doped graphitic carbon nitride nanosheets: experimental and theoretical calculation study. *ACS Sustain. Chem. Eng.* **6**, 10606–10615 (2018).
34. Liang, J., Jiao, Y., Jaroniec, M. & Qiao, S. Z. Sulfur and nitrogen dual-doped mesoporous graphene electrocatalyst for oxygen reduction with synergistically enhanced performance. *Angew. Chem. Int.* **51**, 11496–11500 (2012).
35. Ran, J., Ma, T. Y., Gao, G., Du, X.-W. & Qiao, S. Z. Porous P-doped graphitic carbon nitride nanosheets for synergistically enhanced visible-light photocatalytic H_2 production. *Energy Environ. Sci.* **8**, 3708–3717 (2015).
36. Jourshabani, M., Shariatinia, Z. & Badiei, A. High efficiency visible-light-driven Fe_2O_3-xSx/S-doped g-C_3N_4 heterojunction photocatalysts: Direct Z-scheme mechanism. *J. Mater. Sci. Technol* **34**, 1511–1525 (2018).
37. Cao, S. *et al.* Sulfur-doped g-C_3N_4 nanosheets with carbon vacancies: general synthesis and improved activity for simulated solar-light photocatalytic nitrogen fixation. *Chem. Eng.* **353**, 147–156 (2018).
38. Guo, S. *et al.* Efficient removal of Zn (II), Pb (II), and Cd (II) in waste water based on magnetic graphitic carbon nitride materials with enhanced adsorption capacity. *J. Chem. Eng.* **63**, 3902–3912 (2018).
39. Pourjavadi, A., Hosseini, S. H. & Amin, S. S. Novel high loaded magnetic nanocatalyst based on multi-layered coating of poly (1-vinylimidazole). *Chem. Eng.* **247**, 85–92 (2014).
40. Kara, A. & Erdem, B. Synthesis, characterization and catalytic properties of sulfonic acid functionalized magnetic-poly (divinylbenzene-4-vinylpyridine) for esterification of propionic acid with methanol. *J. Mol. Catal. A* **349**, 42–47 (2011).
41. Takafuji, M., Ide, S., Ihara, H. & Xu, Z. Preparation of poly (1-vinylimidazole)-grafted magnetic nanoparticles and their application for removal of metal ions. *Chem. Mater.* **16**, 1977–1983 (2004).
42. Pekel, N. & Güven, O. Investigation of complex formation between poly (N-vinyl imidazole) and various metal ions using the molar ratio method. *Colloid Polym. Sci.* **277**, 570–573 (1999).
43. Tarley, C. R. T. *et al.* Synthesis and application of imprinted polyvinylimidazole-silica hybrid copolymer for Pb^{2+} determination by flow-injection thermospray flame furnace atomic absorption spectrometry. *Anal. Chim. Acta* **703**, 145–151 (2011).
44. Osman, B., Kara, A., Uzun, L., Beşirli, N. & Denizli, A. Vinyl imidazole carrying metal-chelated beads for reversible use in yeast invertase adsorption. *J. Mol. Catal. B* **37**, 88–94 (2005).
45. Abo-Hamad, A., AlSaadi, M. A., Hayyan, M., Juneidi, I. & Hashim, M. A. Ionic liquid-carbon nanomaterial hybrids for electrochemical sensor applications: a review. *Electrochim. Acta* **193**, 321–343 (2016).
46. Morrison, D. W., Forbes, D. C. & Davis, J. H. Jr. Base-promoted reactions in ionic liquid solvents. The Knoevenagel and Robinson annulation reactions. *Tetrahedron Lett.* **42**, 6053–6055 (2001).
47. Burate, P. A., Javle, B. R., Desale, P. H. & Kinage, A. K. Amino acid amide based ionic liquid as an efficient organo-catalyst for solvent-free Knoevenagel condensation at room temperature. *Catal. Lett.* **149**, 2368–2375 (2019).
48. Sadjadi, S. & Atai, M. Ternary hybrid system of halloysite nanotubes, polyacrylamides and cyclodextrin: an efficient support for immobilization of Pd nanoparticles for catalyzing coupling reaction. *Appl. Clay Sci.* **153**, 78–89 (2018).
49. Sadjadi, S., Heravi, M. M. & Malmir, M. Pd@ HNTs-CDNS-g-C_3N_4: A novel heterogeneous catalyst for promoting ligand and copper-free Sonogashira and Heck coupling reactions, benefits from halloysite and cyclodextrin chemistry and g-C_3N_4 contribution to suppress Pd leaching. *Carbohydr. Polym.* **186**, 25–34 (2018).
50. Sadjadi, S., Malmir, M., Heravi, M. M. & Kahangi, F. G. Magnetic covalent hybrid of graphitic carbon nitride and graphene oxide as an efficient catalyst support for immobilization of Pd nanoparticles. *Inorg. Chim. Acta* **488**, 62–70 (2019).
51. Sadjadi, S., Malmir, M. & Heravi, M. M. Preparation of Ag-doped g-C_3N_4 Nano sheet decorated magnetic γ-Fe_2O_3@ SiO_2 core-shell hollow spheres through a novel hydrothermal procedure: investigation of the catalytic activity for A^3, KA^2 coupling reactions and [3+ 2] cycloaddition. *Appl. Organomet. Chem.* **32**, e4413 (2018).
52. Sadjadi, S. & Koohestani, F. Pd immobilized on polymeric network containing imidazolium salt, cyclodextrin and carbon nanotubes: efficient and recyclable catalyst for the hydrogenation of nitroarenes in aqueous media. *J. Mol. Liq.* **301**, 112414 (2020).
53. Sadjadi, S. & Koohestani, F. Functionalized chitosan polymerized with cyclodextrin decorated ionic liquid: metal free and biocompatible catalyst for chemical transformations. *Int. J. Biol. Macromol.* **147**, 399–407 (2020).
54. Sadjadi, S., Heravi, M. M. & Kazemi, S. S. Ionic liquid decorated chitosan hybridized with clay: a novel support for immobilizing Pd nanoparticles. *Carbohydr. Polym.* **200**, 183–190 (2018).
55. Liu, G. *et al.* Unique electronic structure induced high photoreactivity of sulfur-doped graphitic C_3N_4. *J. Am. Chem. Soc.* **132**, 11642–11648 (2010).
56. Jang, S. *et al.* Recent novel hybrid Pd–Fe_3O_4 nanoparticles as catalysts for various C-C coupling reactions. *Processes* **7**, 422 (2019).
57. Yang, Y. & Tang, R. Magnetically Recyclable Pd/Fe_3O_4/g-C_3N_4 as efficient catalyst for the reduction of nitrophenol and suzuki-miyaura reaction at room temperature. *Chem. Lett.* **47**, 544–547 (2018).
58. Fan, L. *et al.* Chelating capture and magnetic removal of non-magnetic heavy metal substances from soil. *Sci. Rep.* **6**, 21027 (2016).
59. Dorraj, M. *et al.* Enhanced visible light photocatalytic activity of copper-doped titanium oxide–zinc oxide heterojunction for methyl orange degradation. *Appl. Surf. Sci.* **414**, 251–261 (2017).
60. Dorraj, M., Goh, B. T., Sairi, N. A., Woi, P. M. & Basirun, W. J. Improved visible-light photocatalytic activity of TiO_2 co-doped with copper and iodine. *Appl. Surf. Sci.* **439**, 999–1009 (2018).
61. Esmaeili, N., Mohammadi, P., Abbaszadeh, M. & Sheibani, H. Au nanoparticles decorated on magnetic nanocomposite (GO-Fe_3O_4/Dop/Au) as a recoverable catalyst for degradation of methylene blue and methyl orange in water. *Int. J. Hydrog. Energy* **44**, 23002–23009 (2019).

Acknowledgements

The authors gratefully acknowledge the partial support of Iran Polymer and Petrochemical Institute and Iran's National Elites Foundation. Partial help of Dr. P. Mohammadi is also appreciated.

Author contributions

M.D.: Experimental work, writing the draft S.S.: Supervision, Funding, finalizing the manuscript M.M.H.: Financial support.

Competing interests

The authors declare no competing interests.

Additional information

Supplementary information is available for this paper at https://doi.org/10.1038/s41598-020-70457-5.

Correspondence and requests for materials should be addressed to S.S.

Reprints and permissions information is available at www.nature.com/reprints.

Publisher's note Springer Nature remains neutral with regard to jurisdictional claims in published maps and institutional affiliations.